**BLIND DECONVOLUTION THROUGH POLARIZATION DIVERSITY OF
LONG EXPOSURE IMAGERY**

THESIS

Steven P. James, First Lieutenant, USAF
AFIT/EO/ENG/09-06

**DEPARTMENT OF THE AIR FORCE
AIR UNIVERSITY**

AIR FORCE INSTITUTE OF TECHNOLOGY

Wright-Patterson Air Force Base, Ohio

APPROVED FOR PUBLIC RELEASE; DISTRIBUTION UNLIMITED

AFIT/EO/ENG/09-06

**BLIND DECONVOLUTION THROUGH POLARIZATION DIVERSITY OF
LONG EXPOSURE IMAGERY**

THESIS

Presented to the Faculty

Department of Electrical and Computer Engineering

Graduate School of Engineering and Management

Air Force Institute of Technology

Air University

Air Education and Training Command

In Partial Fulfillment of the Requirements for the

Degree of Master of Science

Steven P. James, BS

First Lieutenant, USAF

March 2009

APPROVED FOR PUBLIC RELEASE; DISTRIBUTION UNLIMITED

BLIND DECONVOLUTION THROUGH POLARIZATION DIVERSITY OF LONG EXPOSURE IMAGERY

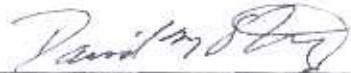Steven P. James, BS
First Lieutenant, USAF

Approved:

Stephen C. Cain (Chairman)

16 March 2009
Date

David M. Strong (Member)

17 March 2009
Date

Richard K. Martin (Member)

17 March 2009
Date

AFIT/EO/ENG/09-06

Abstract

The purpose of the algorithm developed in this thesis was to create a post processing method that could resolve objects at low signal levels using polarization diversity and no knowledge of the atmospheric seeing conditions. The process uses a two-channel system, one unpolarized image and one linearly polarized image, in a GEM algorithm to reconstruct the object. Previous work done by Strong showed that a two-channel system using polarization diversity on short exposure imagery could produce images up to twice the diffraction limit. In this research, long exposure images were simulated and a simple Kolmogorov model used. This allowed for the atmosphere to be characterized by single parameter, the Fried Parameter. Introducing a novel polarization prior that restricts the polarization parameter, it was possible to determine the Fried Parameter to within half a centimeter without any addition knowledge or processes. It was also found that when high polarization diversity was present in the image could be reconstructed with significantly better resolution and signal level did not affect this resolving capability. At very low signal levels, imagery with low to no diversity could not be resolved at all whereas high diversity resolved equally as well as if there was a high signal level. Current algorithms being used do not include polarization diversity but can substantially improve resolution. Application of this algorithm could be used in dim-object detection around satellites as well as solar surface imagery.

Table of Contents

List of Figures

BLIND DECONVOLUTION THROUGH POLARIZATION DIVERSITY OF LONG EXPOSURE IMAGERY

I. Introduction

1.1 Motivation

In 2001 the Department of Defense released a comprehensive report on the United States

Space Capabilities. In that report, it was said that we are ripe for a "Space Pearl Harbor."

[3] Since then, there has been a concerted effort to mitigate this possibly with the

advancement of Space Superiority. This is broken down into three categories: Offensive

Counterspace, Defensive Counterspace, and Space Situational Awareness (SSA). In orbit

around the earth it is very difficult to identify and characterize anomalies that may occur

with "blue" spacecraft or the functions and purpose of "red" spacecraft. That is where

SSA comes in. It is the attempt to have complete awareness of the battlespace in orbit.

Advanced sensors designed to inspect the orbital battlespace or ground-based telescope

systems are required. The design and launch of satellites are very costly, especially at

geosynchronous (GEO) orbit. At Geo, there is so much distance between satellites that

space-based optical systems need to be maneuvered close to each Resident Space Object

(RSO) of interest. This greatly limits lifetime due to finite fuel, and also restricts the

response time kill chain after an event occurs. On the other hand, ground based optical

systems have a comparably low cost, can be easily repaired or upgraded, and can respond

quickly when an event occurs. The drawback is that observing must take place anywhere

from hundreds of kilometers, for low earth, to thousands of kilometers for GEO. On top

of that, resolution is reduced considerable by atmospheric seeing conditions. If large

enough telescopes or telescope arrays are constructed, atmospheric distortion is the main

thing that needs to be mitigated. Adaptive Optics can help significantly with this but do not correct for all atmospheric distortion. Post processing algorithms can be used to further reconstruct the RSO. Combinations of Adaptive Optics and post processing are currently being used operationally to characterize satellites and anomalies in space.

1.2 Goals

1. The purpose of this thesis research is to develop an algorithm that can be used with or without adaptive optics to improve image resolution of space objects through the use of polarization diversity.

2. The algorithm should produce better resolved images when polarization diversity is high.

3. Knowledge of the atmospheric seeing parameter should not be necessary to restore the image and further should be capable of being estimated from a likelihood model.

4. The algorithm should be able to function even at very low signal levels.

1.3 Previous Work

The worked developed in this thesis is built primarily from the research done by Major David Strong [11] and Lieutenant Colonel Adam McDonald [7]. Strong's dissertation created a two-channel, one unpolarized and one linearly polarized, blind deconvolution algorithm for passively illuminated objects as is done in this thesis but with several key differences. His algorithm was created for use in short exposure images as opposed to

long exposure. Details of the object will not be blurred out as much from averaging over a longer period of time. The drawback to the short exposure case is that signal levels are significantly reduced and therefore the SNR is much lower. The other downside to this is that the point spread function (psf) of the atmosphere is not as well known. As an image is integrated, the psf will tend toward a well known and easily modeled transfer function, such as the Kolmogorov spectrum. In contrast, if the integration time is small, fluctuations in the atmosphere can cause the psf to vary greatly. This makes it difficult to estimate and characterize [11].

Another major difference is in the development of the two-channel algorithm derivation. In this thesis, a prior density for the polarization term is included to restrict the possible values that the polarization parameter can take. This allows for the polarization state and the object to be estimated simultaneously. The addition of the prior gives significantly increased information when polarization diversity is present and when calculating the correct seeing parameter of the atmosphere [11:Chap 5].

In MacDonald's work, he developed a method for estimating the seeing parameter of the atmosphere (r_0) for a single channel system of laser light, conforming to a negative binomial distribution. The method involved representing the r_0 probability density function in some distribution. In that case, based on the observation that good seeing (high r_0) is much less likely than bad seeing (low r_0), an exponentially decreasing function was chosen

$$f(r_0) = \frac{N^2}{r_{avg}} e^{-N^2 \frac{r_0}{r_{avg}}} \tag{1.1}$$

where N is the number of pixels on a side and r_{avg} is some parameter that must be iteratively calculated. Once the average seeing parameter is found it produces a graph similar to that in Figure 3.2. When equation (1.1) is left out when deriving the likelihood, there is no decrease around the actual r_0 value and the likelihood continues to increase forever [7:Sect 3.2].

It was assumed that MacDonald's method would be needed to find the correct seeing parameter for the algorithm described in this document. Surprisingly, this was not the case. By using the polarization diversity algorithm with a polarization prior, the likelihood curve naturally produces a maximum near the actual r_0 value. The curve looks very similar to what is produced by Adam MacDonald's iterative method.

1.4 Summary of the Document

Chapter 1: This chapter presents a brief description of what the problem with current Space Situational Awareness capabilities and why it is important that new methods be developed for the Air Force. Along with this, relevant previous work done in blind deconvolution and polarization diversity is discussed.

Chapter 2: This chapter presents the background material necessary to understand the development of the polarization diversity blind deconvolution algorithm. Topics discussed include polarization, linear systems, Fourier optics, atmospheric turbulence, and estimation theory.

Chapter 3: Development of the blind deconvolution algorithm is explained here. Beginning with a two-channel system, Poisson statistics are used to create a likelihood

model. It is further refined by introducing a complete data model. The general method used to estimate the object is the General Expectation Maximization (GEM) algorithm.

Chapter 4: Simulations done using the algorithm and its results are discussed. To quantify how the algorithm performs at varying signal levels and polarizations, two bar targets, polarized differently in the same scene, are propagated through a simulated atmosphere and aperture and then reconstructed.

Chapter 5: This last chapter discusses general conclusions about the functionality and utility of the developed algorithm. Also, further testing and application are mentioned for future work.

II. Background

2.1 Polarimetry

2.1.1 Linearly Polarized Light

Light is an oscillating electromagnetic wave with both an electric field component and a magnetic field component. The entire light wave can be described completely by only the electric field oscillations. Given a cartesian coordinate plane, the total electric field at any point is given by

$$\vec{E}(z,t) = \vec{E}_x(z,t) + \vec{E}_y(z,t) \tag{2.1}$$

With z being the direction of propagation and t is time. This says that the composite electric field is just a superposition of the x and y components of the field. The individual component waves are described by the well known standing wave equation

$$\vec{E}_x(z,t) = E_{x0}\cos(kz - \omega t)\hat{\imath} \tag{2.2}$$

$$\vec{E}_y(z,t) = E_{y0}\cos(kz - \omega t + \epsilon)\hat{\jmath} \tag{2.3}$$

where k is the wave number, ω is the frequency, ϵ is a phase shift between the waves and the scalar E_0 is the magnitude of the field component. Assuming that ϵ is constant, then the total electric field will oscillate linearly at some angle defined by the phase shift. An example of this is shown in figure 2.1. In the case where the phase shift is a multiple of π, the oscillation will be along either the x or y axis. This is called horizontally and
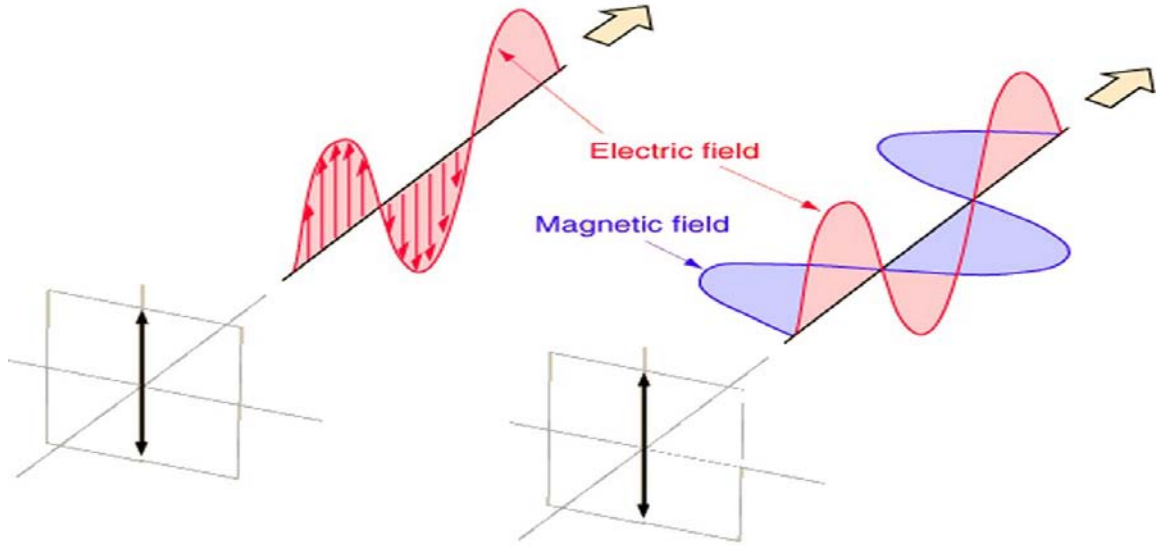
Figure 2.1: The above diagram shows a total oscillating electric field that is vertically polarized. Image taken from George State University Hyperphysics website: http://hyperphysics.phy-astr.gsu.edu/HBASE/phyopt/polclas.html#c1

vertically polarized light, respectively. In the development of this thesis, only linearly polarized light is considered so elliptical polarization will not be discussed [9:280-285].

2.1.2 Unpolarized Light Sources

The term "natural light" refers to a source that is completely unpolarized. However, it is not that the light is unpolarized, it is that the light is changing its polarization state so quickly that it cannot be determined. When excited electrons in an atom return to a lower energy state, that energy is released via a photon of light. The electric field orientation of the emitted photon can be thought of as random, even though it is determined by the angular momentum of the system. Photon fluxes can vary greatly but are usually on the order of $10^{20} s^{-1}$. With such a large number of constantly changing polarizations, natural light can easily be considered random [9:280-285].

7

2.1.3 Polarization State

For this thesis, only one polarization parameter is needed. That is the total linear polarization state, P, of the observed light. As discussed in the previous section, natural light is unpolarized. When that light is integrated over time and decomposed into its x and y components, one would expect to find half of the light to be horizontally polarized and the other half to be vertically polarized. The ratio of one of those components to the total light collected is P. It is unimportant which component since they are compliments of each other and coordinate system can be rotated arbitrarily in the x-y plane. In order to use the polarization diversity algorithm, one channel collects light directly off the telescope and the other channel utilizes a linear polarizer in front of the CCD. The orientation of the polarizer does not matter since the x-y coordinate system chosen is completely arbitrary.

When natural light is reflected off an object, it can become polarized by the material the object is composed of. The amount of polarization is dependent on material characteristics and the geometry of the scene. Manmade objects tend to polarize light upon reflection very strongly as do sharp edges.

2.2 Diffraction

2.2.1 Linear System Theory & The Transfer Function

Linear systems are those that produce a response to a collection of inputs equal to the sum of the responses obtained from the inputs if they were applied individually. These types of transformations can be found in many places, most notably in the time domain

for electronic circuits and in the spatial domain for optical systems. A transformation

operator, L, is considered to be linear if it obeys the following mathematical property,

defined as superposition

$$\text{L}\{ap(x) + bq(x)\} = a\text{L}\{p(x)\} + b\text{L}\{q(x)\} \tag{2.4}$$

where *a* & *b* are scalar quantities and *p(x)* & *q(x)* are input functions. *x* represents an

arbitrary coordinate system, be it time, space, frequency, etc… This superposition

definition has some important properties to note. First, a linear system is unaffected by

the scalar magnitude of a function it is operating on. Secondly, the sum of the output

functions is equal to the output of the sum of the functions; meaning that there is no

"mixing" between functions when the operator acts on several at one time. To see how

this applies to an optical system, the quantities of equation (2.4) must be given physical

definition [6:19].

The input function is a function of the light that leaves the object. It has not passed

through any optics or been aberrated in any way. The output function is the image

obtained by the camera. The linear process that is applied to the object is the actual

propagation of the light through the atmosphere and optical system. To understand the

form of the linear transformation, the impulse response of the system must be found. It is

assumed known that if a linear operator is applied to an impulse, the output is the

characteristic response of the system. Mathematically, an impulse can be described by a

delta function, $\delta(x)$. Application of the sifting property yields

$$p_1(x_2) = \iint\limits_{-\infty}^{\infty} p_1(x_1)\delta(x_2 - x_1)dx_1 \tag{2.5}$$

Again, x_1 and x_2 are two-dimensional coordinates and p_1 is object function. If the operator, L, is applied to this with respect to the x_2 coordinate space, one gets

$$p_2(x_2) = L\{p_1(x_2)\} = \iint\limits_{-\infty}^{\infty} p_1(x_1)L\{\partial(x_2 - x_1)\}dx_1 \qquad (2.6)$$

As mentioned above, the impulse response is defined as the output of a linear operator as applied to a single impulse. This will be given the definition

$$h(x_2 - x_1) = L\{\partial(x_2 - x_1)\} \qquad (2.7)$$

substituting this back into equation (2.6) obtains

$$p_2(x_2) = \iint\limits_{-\infty}^{\infty} p_1(x_1)h(x_2 - x_1)dx_1 \qquad (2.8)$$

This is a general convolution integral between the original object function and the impulse response. Convolutions are almost always computationally intense and difficult to calculate. If this is done in the spatial frequency domain, the two functions can simply be multiplied together and then the inverse Fourier transform taken such that

$$p_2(x_2) = \mathcal{F}^{-1}\{P_1(f_{x_1})H(f_{x_1})\} \qquad (2.9)$$

$P_1(f_{x_1})$ and $H(f_{x_1})$ are the Fourier transforms of $p_1(x_1)$ and $h(x_2 - x_1)$, respectively. $\mathcal{F}^{-1}\{\}$ is the inverse Fourier transform operator. Specifically, $H(f_{x_1})$ is called the Transfer Function of the system and is defined as [6:19-21]

$$H(f_x, f_y) = \int\int_{-\infty}^{\infty} h(x, y) e^{-i2\pi(f_x x + f_y y)} dx dy \qquad (2.10)$$

2.2.2 The Point Spread Function

A delta function was used to define the impulse response of the system. In imaging applications, the impulse response is also referred to as the Point Spread Function (psf). In terms of an optical system, the best way to model the psf is to use a completely black, zero intensity image with one pixel at the center having a maximum intensity. It is not a perfect delta function for the continuous case but is in a discrete model, such as an array of pixels. It represents an image with infinite frequency content, meaning that its Fourier transform does not go to zero as frequency increases [6:20-21].

If this point source is propagated through an aperture, the psf is found and therefore the transfer function is also known for the system. Figure 2.3 shows both the object and the observed image for several circular apertures. As the images show, the point source becomes more and more spread out as the aperture size decreases. This loss in definition can be explained by the transfer function. The size of the aperture determines the maximum spatial frequencies that can be recovered. Since a point source contains infinite frequency content, it gets blurred out due to the aperture cutting off higher spatial

11

frequencies. Looking at the transfer functions in Figure 2.4, it is clear that as the aperture

shrinks, so does the cutoff frequency.

1.56cm point, 100cm window   Optic = 32cm   Optic = 25cm   Optic = 20cm

Optic = 15cm   Optic = 10cm   Optic = 5cm   Optic = 2cm
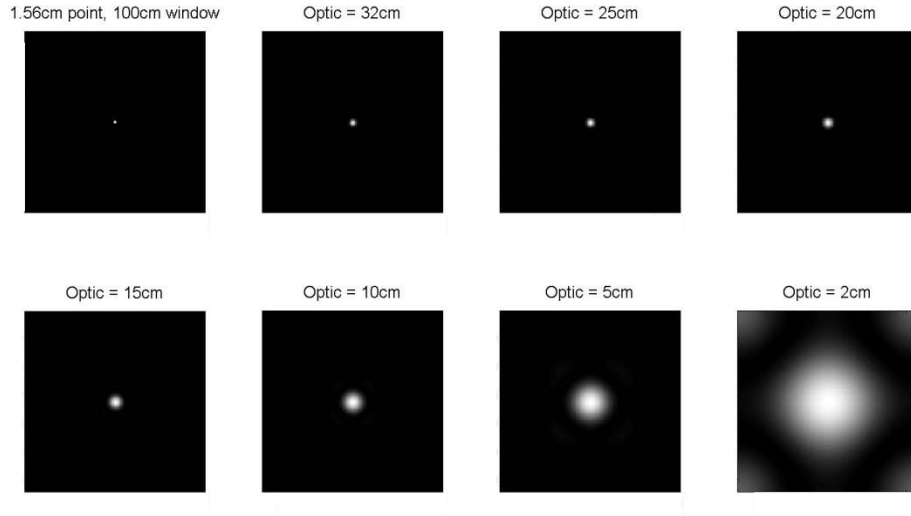
Figure 2.2: The first image is that of the original object with a square window of 100cm^2. Each successive image is the object propagated through a circular aperture of the diameter specified.

Optic = 20cm   Optic = 15cm   Optic = 5cm   Optic = 2cm
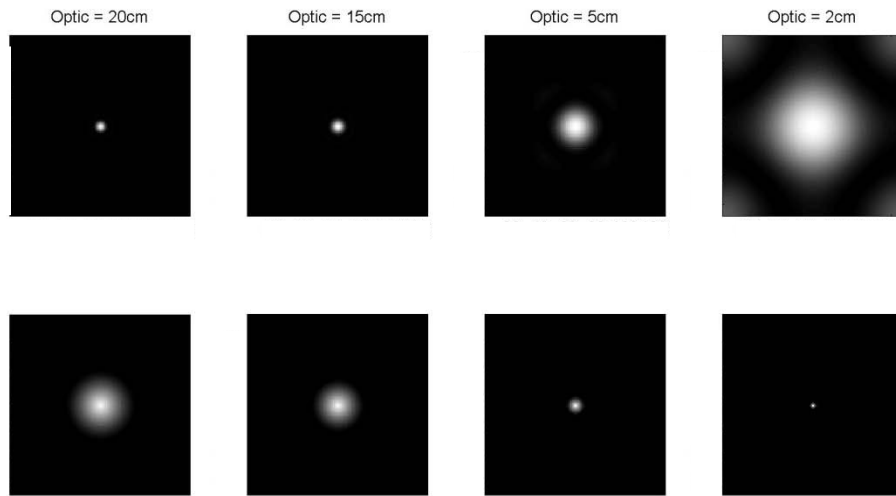
Figure 2.3: The top row shows the image of a point source as seen through a circular aperture of the given diameter. Directly below each image is the transfer function. The transfer function is in spatial frequency. As the diameter shrinks, so does the maximum spatial frequency.

12

2.3 Turbulence

2.3.1 The Long Exposure Optical Transfer Function

The algorithm developed in this thesis is based on the Long Exposure Optical Transfer Function (LEOTF) for a combined atmosphere-optics system. Over any integration time, the optics of the telescope do not change but the atmosphere is in a constant state of turbulent change. To find the LEOTF of the entire system, the derivation begins with the definition of an OTF

$$\mathcal{H}(v_u, v_v) = \frac{\iint_{-\infty}^{\infty} H(x,y)H^*(x - \bar{\lambda}fv_u, y - \bar{\lambda}fv_v)dxdy}{\iint_{-\infty}^{\infty}|H(x,y)|^2 dxdy} \tag{2.11}$$

where $\bar{\lambda}$ is the mean wavelength, f is the effective focal length of the optical system, and v_u and v_v are the spatial frequency coordinates for the Fourier transform space in the image plane [6:139-140]. For the long exposure case the atmosphere can be condensed into a single phase screen located directly in front of the aperture. With this simplification

$$H(x,y) = P(x,y)e^{i\theta(x,y)} \tag{2.12}$$

in which $P(x,y)$ is the pupil function and θ is a random Gaussian variable with mean equal to zero [6:145-147]. Inserting this into equation (2.11) and taking the expectation, the equation becomes

$$\bar{\mathcal{H}}_{sys}(v_u, v_v) = E\left[\frac{\iint_{-\infty}^{\infty} P(x,y)P^*(x - \bar{\lambda}fv_u, y - \bar{\lambda}fv_v)e^{i\theta(x,y)}e^{-i\theta(x-\bar{\lambda}fv_u,y-\bar{\lambda}fv_v)}dxdy}{\iint_{-\infty}^{\infty}|P(x,y)|^2 dxdy}\right] \tag{2.13}$$

where θ is a random phase for the light coming through the pupil. In the denominator, the phase of the transfer function is the same as the conjugate transfer function so they cancel out; however, this is not true for the numerator. The only random quantity in equation (2.13) is the phase so the expectation can be brought inside upper integrals yielding

$$\overline{\mathcal{H}}_{sys}(v_u, v_v) = \frac{\iint_{-\infty}^{\infty} P(x,y)P^*\left(x - \bar{\lambda}fv_u, y - \bar{\lambda}fv_v\right)E\left[e^{i\,\theta'}\right]dxdy}{\iint_{-\infty}^{\infty}|P(x,y)|^2 dxdy} \tag{2.14}$$

with the variable substitution $\theta' = [\theta(x,y) - \theta(x - \bar{\lambda}fv_u, y - \bar{\lambda}fv_v)]$ made. In order to determine a usable form of the expectation, the characteristic function is needed. It is defined as

$$\Phi_{\theta'}(\omega) = E[e^{i\omega\theta'}] \tag{2.15}$$

where ω is Fourier transform variable associated with the frequency content of θ'. This is similar to equation (2.14) which has $\omega = 1$. Since both $\theta(x,y)$ and $\theta\left(x - \bar{\lambda}fv_u, y - \bar{\lambda}fv_v\right)$ are Gaussian random variables, θ' is also Gaussian. The characteristic function for a zero mean Gaussian is given by,

$$\Phi_{\theta'}(\omega) = e^{\frac{\sigma^2\omega^2}{2}} \tag{2.16}$$

where σ^2 is the variance of the variable θ'. Setting $\omega = 1$ and inserting this equivalent form into equation (2.14) then pulling it outside the integrals it becomes

$$\overline{\mathcal{H}}_{sys}(v_u, v_v) = \left(e^{\frac{\sigma^2}{2}}\right)\left(\frac{\iint_{-\infty}^{\infty} P(x,y)P^*\left(x - \bar{\lambda}fv_u, y - \bar{\lambda}fv_v\right)dxdy}{\iint_{-\infty}^{\infty}|P(x,y)|^2 dxdy}\right) \tag{2.17}$$

$$\sigma^2 = E\left[\{\theta(x,y) - \theta\left(x - \bar{\lambda}f\nu_u, y - \bar{\lambda}f\nu_v\right)\}^2\right] = 2\sigma_0^2 - 2E[\theta(x,y)\theta\left(x - \bar{\lambda}f\nu_u, y - \bar{\lambda}f\nu_v\right)] \qquad (2.18)$$

where σ^2 is the variance of the phase difference. Equation (2.18) gives the definition of the variance and then puts it in terms of correlations. This is called a phase structure function. The first term in equation (2.17) is only dependent on the phase delays caused by the atmosphere and the second term is just the OTF of the optical system alone which is written as

$$\bar{\mathcal{H}}_{atm}(\nu_u, \nu_v) = e^{\frac{\sigma^2}{2}} \qquad (2.19)$$

$$\mathcal{H}_0(\nu_u, \nu_v) = \frac{\iint_{-\infty}^{\infty} P(x,y)P^*\left(x - \bar{\lambda}f\nu_u, y - \bar{\lambda}f\nu_v\right)dxdy}{\iint_{-\infty}^{\infty}|P(x,y)|^2 dxdy} \qquad (2.20)$$

This demonstrates that the LEOTF of the entire system is completely separable with respect to the atmosphere and optics [5:404-407]

$$\bar{\mathcal{H}}_{sys}(\nu_u, \nu_v) = \bar{\mathcal{H}}_{atm}(\nu_u, \nu_v)\mathcal{H}_0(\nu_u, \nu_v) \qquad (2.21)$$

2.3.2 Phase Structure Function

One way to characterize the statistical correlation between two points in a distribution is through the structure function. The structure function can be described as the variance of the difference between two points in a field. For the case of the phase difference the structure function looks like

$$D(x, y, \Delta x, \Delta y) = E[\{\theta(x + \Delta x, y + \Delta y) - \theta(x, y)\}^2] \tag{2.22}$$

where x and y are general spatial coordinates and Δx and Δy are deviation for the coordinates. At this point, the structure function could be substituted into equation (2.19) in place of the variance term. However, just a few more steps will be performed before this is done. If the square term is multiplied out and the expectation broken up of these terms it gives

$$D(x, y, \Delta x, \Delta y) = E[\theta^2(x + \Delta x, y + \Delta y)] + E[\theta^2(x, y)] - 2E[\theta(x + \Delta x, y + \Delta y)\theta(x, y)] \tag{2.23}$$

The above string of expectations can be expressed in terms of the correlation function eliminating the need for an initial (x, y) coordinate. This now describes the structure function as

$$D_\theta(\Delta x, \Delta y) = 2[R_\theta(0,0) - R_\theta(\Delta x, \Delta y)] \tag{2.24}$$

Lastly, this structure function can be inserted into equation (2.19) giving an average atmospheric transfer function in terms of autocorrelations [1:38-40]

$$\overline{\mathcal{H}}_{atm}(\nu_u, \nu_v) = e^{\frac{-D_\theta(\Delta x, \Delta y)}{2}} = e^{-[R_\theta(0,0) - R_\theta(\Delta x, \Delta y)]} \tag{2.25}$$

2.3.3 Kolmogorov Structure Function

The fluctuations in phase are caused by changes in the index of refraction in the air. These changes arise from fluctuations in temperature, and to a lesser degree pressure.

In 1961, Kolmogorov derived an expression for the phase structure function. This is given by

$$D(r) = 2.91k^2 r^{\frac{5}{3}} z C_n^2(z) \qquad (2.26)$$

where k is the wave number, z is the height of the atmospheric turbulence, and C_n^2 is a measure of the strength of atmospheric turbulence, in units of $length^{-2/3}$. Equation (2.26) is for the case of constant C_n^2 [5:413]. If the strength is changing with altitude the structure function is [5:428]

$$D(r) = 2.91k^2 r^{5/3} \int_0^z C_n^2(z') dz' \qquad (2.27)$$

A parameter to describe atmospheric seeing is

$$r_0 \overset{\text{def}}{=} 0.185 \left[\frac{\bar{\lambda}^2}{\int_0^z C_n^2(z') dz'} \right]^{3/5} \qquad (2.28)$$

r_0 is called the Fried Parameter and can be thought of as an average atmospheric coherence length [5:431]. Rearranging this definition and replacing the integral in the structure function, it is written as

$$D(r) = 6.88 \left(\frac{r}{r_0} \right)^{5/3} \qquad (2.29)$$

Finally, this structure function can be inserted into the equation (2.25) yielding the result

$$\bar{\mathcal{H}}_{atm}(v_u, v_v) = e^{-3.44 \left(\frac{r}{r_0} \right)^{5/3}} \qquad (2.30)$$

17

So, the average OTF of the atmosphere can be completely characterized by a single

length parameter, r_0 [5:439].

2.4 Detection

The detection of photons by a detector array is a Poisson process. In this case, an event

will be defined as an individual pixel detecting a photon. For this example, it will be

assumed that the quantum efficiency and photomultiplier are equal to 1. Over some

period of time, either an event does or does not occur with some probability. A binomial

distribution could be used to model this. However, photon events occur in such large

number that the number of trials can be assumed to be infinite. In that case, the

probability of detection is given by a Poisson distribution,

$$G = \frac{i(y)^{k(y)} e^{-i(y)}}{k(y)!} \tag{2.31}$$

where $i(y)$ is the mean number of events and $k(y)$ is the number of successes [5:466-

467]. For an imaging system, the mean number of events is given by estimated image

intensity, $i(y)$, and k is the photocount data. For multiple pixels, the composite pdf of the

entire array, assuming statistical independence between detector measurements, is

$$G = \prod_y^Y \frac{i(y)^{d(y)} e^{-i(y)}}{d(y)!} \tag{2.32}$$

18

where y is actually a two dimensional variable representing the image plane, Y is the

dimensions of that image plane, and $d(y)$ is the data [10:1065]. How the model

describes the intensity of the image will be discussed in chapter 3.

III. Algorithm Design

3.1 Log-Likelihood Data Model

3.1.1 Incomplete Data

As discussed in section 2.4, for photons incident on a detector, a Poisson distribution is used to model the random arrival times of the light. If you now consider the case of an imaging system where two channels are statistically independent, the combined PMF is just the multiplication of the two individual PMFs. This incomplete data likelihood model takes the form

$$G = \prod_{y_1}^{Y_1} \left[\left(\frac{i_{UP}(y_1)^{\tilde{d}_{UP}(y_1)} e^{-i_{UP}(y_1)}}{\tilde{d}_{UP}(y_1)!} \right) \right] \prod_{y_2}^{Y_2} \left[\left(\frac{i_P(y_2)^{\tilde{d}_P(y_2)} e^{-i_P(y_2)}}{\tilde{d}_P(y_2)!} \right) \right] \qquad (3.1)$$

where y_1 and y_2 are general coordinates of the image planes, Y_1 and Y_2 are the total number of pixels, and $\tilde{d}(y)$ is the collected photon counts from the detectors. For reasons discussed below, the data will be referred to as the incomplete data. The subscript UP denotes the unpolarized channel and the subscript P denotes the polarized channel. $i_{UP}(y)$ and $i_P(y)$ are the average intensity of the images given by the convolutions

$$i_{UP}(y_1) = \sum_x^X O(x)h(y_1 - x) \qquad (3.2a)$$

$$i_P(y_2) = \sum_x^X O(x)P(x)h(y_2 - x) \qquad (3.2b)$$

20

$O(x)$ is the object, $h(y - x)$ is the point spread function, $P(x)$ is the set of polarization

states with values between 0 and 1, and x is a general coordinate for the object plane

[10:1065].

3.1.2 Complete & Incomplete Data Relationship

At this point the concept of complete data will be introduced. Complete and incomplete

data are related but the relation between the two can be totally user defined. Further, the

complete data do not even need to be physical. The only requirement is that they be

statistically consistent. It is more a matter of choosing parameters that make the

equations solvable. In this case, the relation between the two will be defined as

$$\tilde{d}(y) = \sum_x^X d(y|x) \tag{3.3}$$

where $d(y|x)$ is a piece of complete data and will be considered a Poisson random

variable. This is saying that the incomplete data is the sum of small individual pieces of

complete data. Since the incomplete data is a sum over a set of Poisson random

variables, it is also a Poisson random variable and remains statistically consistent. The

expectation of the complete data is given by

$$E[d(y|x)] = h(y - x)O(x) \tag{3.4}$$

So, taking the expectation of equation (3.3) and inserting equation (3.4)

$$E[\tilde{d}(y)] = \sum_x^X E[d(y|x)] = \sum_x^X h(y-x)O(x) \tag{3.5}$$

Now the complete data has a relationship to the incomplete data and is statistically

consistent [10:1067].

3.1.3 Complete Data Log-Likelihood

Taking the log of equation (3.1) and assuming statistical independence of the pixels in the

images, the incomplete data log-likelihood is

$$\begin{aligned}
L_{ID} = \sum_y^Y \{\tilde{d}_{UP}(y) \ln\left(\sum_x^X O(x)h(y-x)\right) - \sum_x^X O(x)h(y-x) - \ln(\tilde{d}_{UP}(y)!) + \\
\tilde{d}_P(y) \ln\left(\sum_x^X O(x)P(x)h(y-x)\right) - \sum_x^X O(x)P(x)h(y-x) - \ln(\tilde{d}_P(y)!)\}
\end{aligned} \tag{3.6}$$

The subscript ID stands for incomplete data. This is only shown here for comparison to

the complete data log-likelihood. There is no way to go directly from the incomplete to

the complete data model. The complete data log-likelihood is given by

$$\begin{aligned}
L_{CD} = \sum_y^Y \sum_x^X \{d_{UP}(y) \ln\big(O(x)h(y-x)\big) - O(x)h(y-x) - \ln(d_{UP}(y)!) + \\
d_P(y) \ln\big(O(x)P(x)h(y-x)\big) - O(x)P(x)h(y-x) - \ln(d_P(y)!)\}
\end{aligned} \tag{3.7}$$

This looks very similar to equation (3.6) but there is no direct relationship between them.

The factorial of the data has no terms for $O(x)$ or $P(x)$ and will not affect the likelihood

so they can be dropped. Removing these terms (3.7), it becomes

22

$$L_{CD} = \sum_{y}^{Y}\sum_{x}^{X}\{d_{UP}(y)\ln\big(O(x)h(y-x)\big) - O(x)h(y-x) +$$
$$d_{P}(y)\ln\big(O(x)P(x)h(y-x)\big) - O(x)P(x)h(y-x)\}$$

(3.8)

3.1.1 Polarization Prior

In order to completely describe the joint likelihood of the two channel system, a prior is

needed to constrain the polarization parameters $P(x)$. Right now, the polarization can be

any number greater than or equal to zero, due to the Poisson nature of the signal. It is

known that the value of P cannot exceed 1. Since the likelihood only needs to be limited

by the upper bound, a simple "super-Gaussian" can be used. For the pdf, this would be

$$f(P(x)) = Ae^{-P(x)^{n}}, P(x) \geq 0$$

(3.9)

where n is an even integer and A is a normalizing factor so that the pdf integrates to unity.

The normalizing term is unimportant since once the natural log is taken, it becomes

another constant offset like the data factorial. As n increases, the pdf models a step

function more and more. Figure 3.1 shows a plot of this prior demonstrating how

increasing n approaches a step function. Its purpose is to keep the likelihood low for P

values greater than one but high for values less than one, allowing the data to accurately

estimate the P state. For example, $P = 0.95$, the prior would bias the estimated value

away from this. Now the complete data log-likelihood function is

$$L_{CD} = \sum_{y}^{Y}\sum_{x}^{X}\{d_{UP}(y)\ln\big(O(x)h(y-x)\big) - O(x)h(y-x) +$$
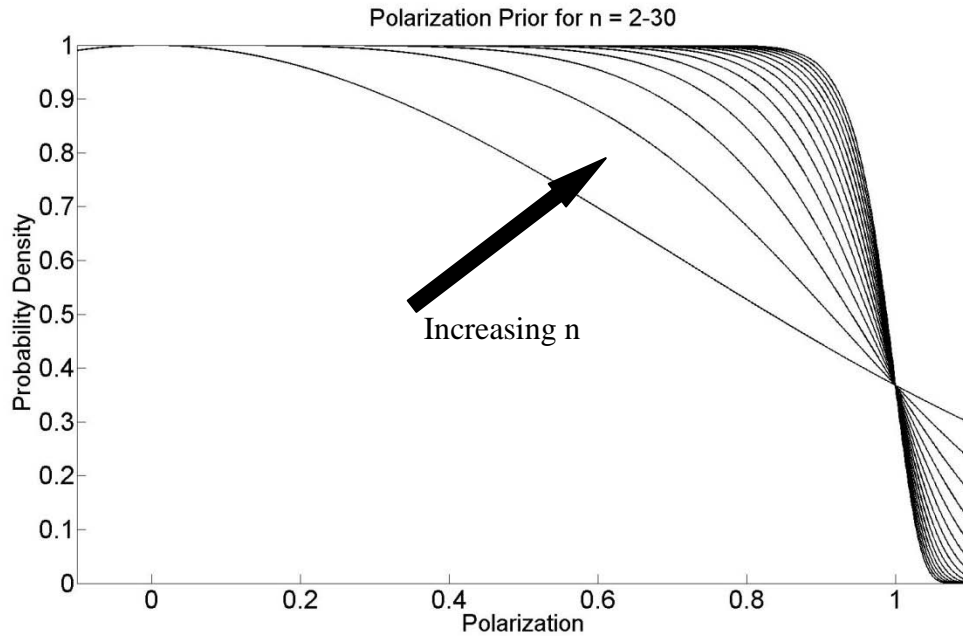$$d_{P}(y)\ln\big(O(x)P(x)h(y-x)\big) - O(x)P(x)h(y-x) - P(x)^{n}\}$$

(3.10)

Figure 3.1: A plot of the prior function in equation (3.9). As *n* increases, the prior models a step function more closely.

3.2 Expectation Maximization Algorithm

The General Expectation Maximization (GEM) algorithm is a method for estimating an unknown quantity, the complete data, given a set of related known quantities, the incomplete data. The process involves taking the conditional expectation of the complete data likelihood given the incomplete data and the old parameter estimates. Once that is done, the final step involves maximizing the new function for the desired parameters. The steps for the GEM algorithm follow the simple format of:

1. Take the conditional expectation of the complete data log-likelihood

2. Maximize the new equation from step 1 for the parameter(s) of interest

3. Calculate the conditional expectation given the old parameters

4. Calculate what the new parameters will be given step 3

5. Iteratively repeat steps 3 and 4 until a stopping criteria is reached

24

3.2.1 Expectation Step

Using the complete data log-likelihood model described earlier in the chapter, a new function can be found by taking the conditional expectation. The general Q function is given as [10:1066]

$$Q\big(O(x), h(y-x)\big) = E[L_{CD}(O(x), h(y-x))|\tilde{d}(y)]$$

(3.11)

The Q function for the likelihood model in equation (3.10) is then

$$Q = E\Big[\sum_{y}^{Y}\sum_{x}^{X}\{d_{UP}(y)\ln\big(O(x)h(y-x)\big) - O(x)h(y-x) + d_{P}(y)\ln\big(O(x)P(x)h(y-x)\big) - O(x)P(x)h(y-x) - P(x)^{n}\}\Big]$$

(3.12)

From this point forward, the conditions of the expectation will be suppressed but should be kept in mind. The conditional expectation can be brought inside the summation. However, the only term within the Q function that is a random variable is the data. Making this simplification, the Q function becomes

$$Q = \sum_{y}^{Y}\sum_{x}^{X}\{E[d_{UP}(y)]\ln\big(O(x)h(y-x)\big) - O(x)h(y-x) + E[d_{P}(y)]\ln\big(O(x)P(x)h(y-x)\big) - O(x)P(x)h(y-x) - P(x)^{n}\}$$

(3.13)

The expectation of the complete data is not a known quantity and must be calculated. A method for calculating the expected value of the data is given by Schulz and used in the previous work done by Strong [11:Chap 5],[10:1067]. Those equations are

$$E[d_{UP}(y)] = \frac{h(y-x)O(x)}{i_{UP}(y|O, h)}\tilde{d}_{UP}(y)$$

(3.14a)

$$E[d_P(y)] = \frac{h(y-x)P(x)O(x)}{i_P(y|O,P,h)} \tilde{d}_P(y) \tag{3.14b}$$

It has been shown that that the conditional probability distributions needed to compute

the conditional expectations in equations (3.14) are binomial [4]. Accepting this, an

intuitive way of thinking about these equations is to remember that the expectation of a

binomial distribution is n times p, where n is the number of trials and p is the probability

of success. The data are a measure of the number of photons that hit a pixel and can be

thought of as n trials. The numerators in the equations are simply a piece of complete

data. In the denominator, the intensity is a sum over all pieces of complete data. So, the

ratio of these two terms is a probability, p.

3.2.2 Maximization Step

In the maximization step, there are two parameters of interest, the object, $O(x)$, and the

polarization state, $P(x)$. These are solved for simultaneously by taking the derivative

with respect to each and setting them equal to zero. First, taking the derivative of the Q

function with respect to $P(x_0)$ and setting equal to zero gives

$$0 = \sum_{y}^{Y} \left\{ \frac{E[d_P(y)]}{P(x_0)} - O(x_0)h(y-x_0) - nP(x_0)^{n-1} \right\} \tag{3.15}$$

Note that the derivative was taken with respect to a specific instance of x so the

summation over the object plane vanishes. The object in the second term is not

dependent on y, only on the psf. By definition, assuming and ideal optical system, the

sum of the psf is equal to 1. Including this and solving for $O(x_0)$ the maximization becomes

$$O(x_0) = \frac{\sum_y^Y E[d_p(y)]}{P(x_0)} - \sum_y^Y nP(x_0)^{n-1} \tag{3.16}$$

This is as far as this equation needs to be simplified. Now to repeat this procedure with respect to the object, $O(x_0)$. Taking the derivative and setting equal to zero, the maximization is

$$0 = \sum_y^Y \left\{ \frac{E[d_{UP}(y)]}{O(x_0)} - h(y - x_0) + \frac{E[d_P(y)]}{O(x_0)} - P(x_0)h(y - x_0) \right\} \tag{3.17}$$

Again, summing over the psf terms and solving for $O(x_0)$, the final form is

$$O(x_0) = \frac{\sum_y^Y E[d_{UP}(y)] + \sum_y^Y E[d_P(y)]}{1 + P(x_0)} \tag{3.18}$$

To remove $O(x_0)$, equations (3.16) and (3.18) are set equal to each other,

$$\frac{\sum_y^Y E[d_{UP}(y)] + \sum_y^Y E[d_P(y)]}{1 + P(x_0)} = \frac{\sum_y^Y E[d_p(y)]}{P(x_0)} - \sum_y^Y nP(x_0)^{n-1} \tag{3.19}$$

Moving all terms to one side and separating them gives

$$0 = -\frac{\sum_y^Y E[d_{UP}(y)]}{1 + P(x_0)} - \frac{\sum_y^Y E[d_P(y)]}{1 + P(x_0)} - \sum_y^Y d_p(y) - \sum_y^Y nP(x_0)^{n-1} \tag{3.20}$$

27

The last step is to multiply through by $-(1 + P(x_0))$ which shows that

$$0 = nP(x)^{n+1} + nP(x)^n + P(x) \sum_y^Y E[d_{UP}(y)] - \sum_y^Y E[d_P(y)] \qquad (3.21)$$

At this point, the only way to solve for $P(x)$ is to find the roots of this polynomial expression. As mentioned before, as n grows larger, the more accurately the prior models a step function. The drawback to a large n is that it requires more computing time. There is only one real root to the expression, but which one it is can't be known prior to solving for them all. A practical value to choose for n would be a number less than 10.

In the algorithm, once $P(x)$ is estimated, it is inserted back into equation (3.18). Then, an estimate for the object can be found. Having a new object and polarization state, the algorithm is looped so that a new intensity and complete data expectation can be calculated to find the next $P(x)$ and $O(x)$ estimates. The iteration process is repeated until the stopping criterion is reached.

3.2.3 Stopping Criterion

In order to know when the algorithm should be stopped, a specific criterion needs to be set. One way to do this is to use the statistical properties of the noise. The intensity is a convolution of the estimated object with the total system transfer function; in effect, it tries to mimic the data. However, the recreated object cannot exactly account for the random noise in the system. So, once the variance difference between the intensity image and the data comes within one standard deviation of the data's variance, the algorithm is

stopped. If it were allowed to iterate beyond this point, the reconstruction will try to incorporate too much of the noise as part of the object, skewing the object estimate. The stopping criterion is then [8]

$$\sigma_p^2 \leq \sum_y^Y \left[\tilde{d}_p(y) - i_p(y)\right]^2 \qquad (3.22)$$

The polarized data set is used instead of the unpolarized because the variance is of the polarized image is always less and the algorithm will converge faster. In test runs of the algorithm, when the unpolarized data was used, the estimated object was noticeably over-iterated.

3.3 Seeing Parameter Estimation

The true seeing parameter r_0 value, which is used to generate the psf, is not known when the algorithm is initialized. The reconstruction is simply recalculated for a range of r_0 values. The likelihood of the reconstructed image is found each time by using equation (3.8). After processing is done, a likelihood curve vs. r_0 values can be plotted. In all cases tested, this plot looks similar to Figure 3.2. The likelihood sharply rises from very bad seeing to the correct r_0 value. This gives a maximum near the actual seeing parameter. The likelihood value itself is not important; it is simply a comparative measure between different r_0 values. The algorithm has a tendency to slightly overestimate r_0 but is usually within a half centimeter of truth.
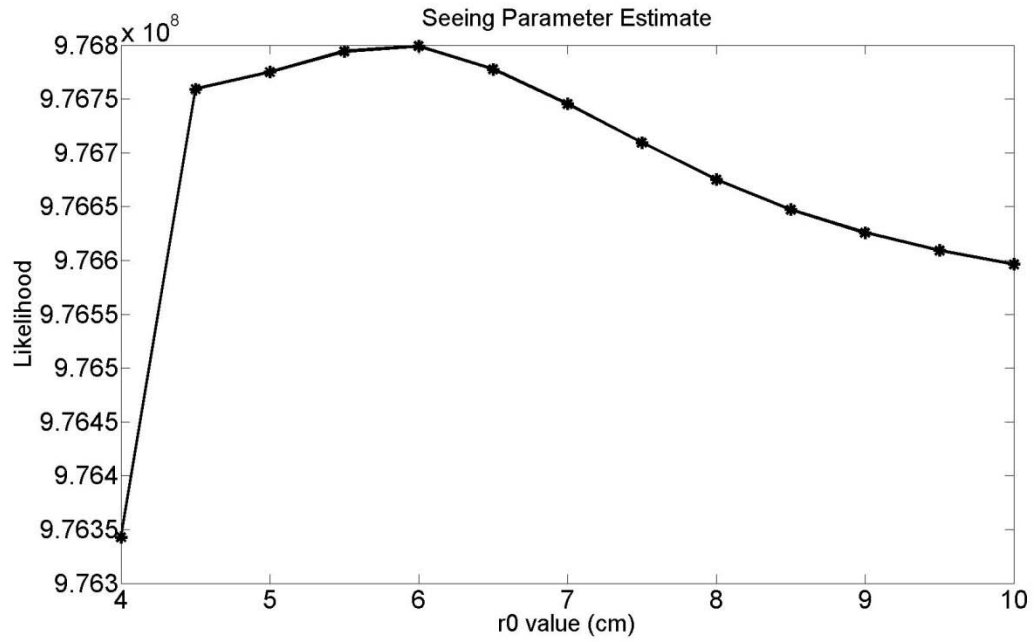
Figure 3.2: After the algorithm produces an estimated image for a range of r_0 values, the likelihood is calculated and plotted. It reaches maximum at or near the true seeing parameter. In this case, the r_0 value was 6cm and was estimated exactly.

IV. Results

4.1 Simulation Setup

In order to accurately quantify the capabilities of the polarization diversity algorithm, a simple object is needed to be reconstructed. It is not as impressive as using satellite images but will provide substantially more information about the bounds of the algorithm. Two bar targets separated by two pixels are used as the object. The total image size used is 60cm on a 64x64 pixel grid so each pixel represents 0.94cm. This object is shown if Figure 4.1. Each bar is set with a different polarization state. The following sections describe the tests that were done on the bar target by varying different parameters of the data.
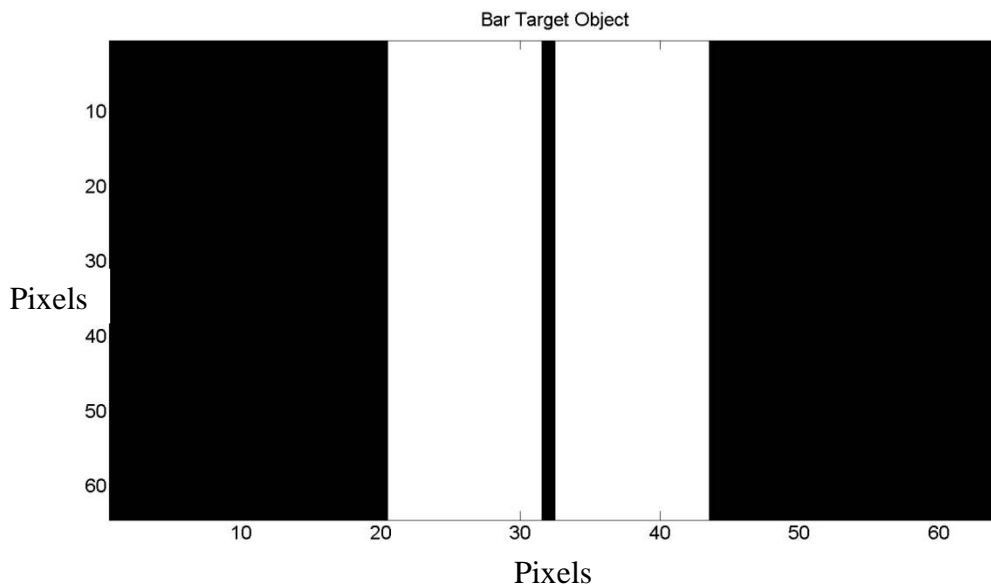

Figure 4.1: Two bars to be propagated through a simulated atmosphere and telescope aperture. Each bar is given a different polarization parameter.

4.2 Test One: Signal Variation

The first simulations were done by varying the polarizations on both bars and also increasing the signal strength of the data. *P* for both bars was iterated from 0 to 1 in 0.1 steps separately. Once there was an object estimate for all possible polarization combinations, the signal power was increased and the process was repeated.

To keep data sizes small, a one-dimensional slice is taken for each estimated object, since the object is uniform in the vertical dimension. If the object were reconstructed perfectly, it would look like two periods of a square wave, as in Figure 4.2. In order to do that though, infinite frequency content would be required in the continuous case. Unfortunately too much of the higher spatial frequencies are lost through diffraction. However, the goal of this simulation is not to exactly reproduce the bar targets but rather just to distinguish that there are two targets present. An example of the reconstructed object is shown in Figure 4.3. It should be noted that the intensity of the image is much higher than that of the object. This does not matter as they are both scaled to the same intensity range when displayed. Figure 4.4 is a screenshot of the algorithm in progress for bar polarizations of 0.2 and 1.0. The top two images are that of the observed data channels after being propagated through the atmosphere and aperture. The bottom right is the object and the bottom left is the reconstruction.
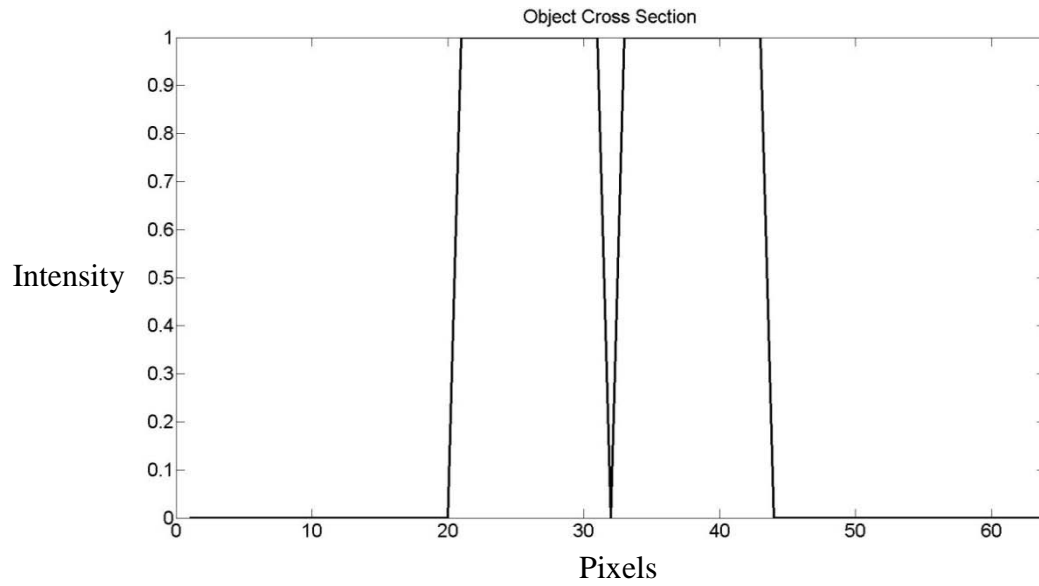
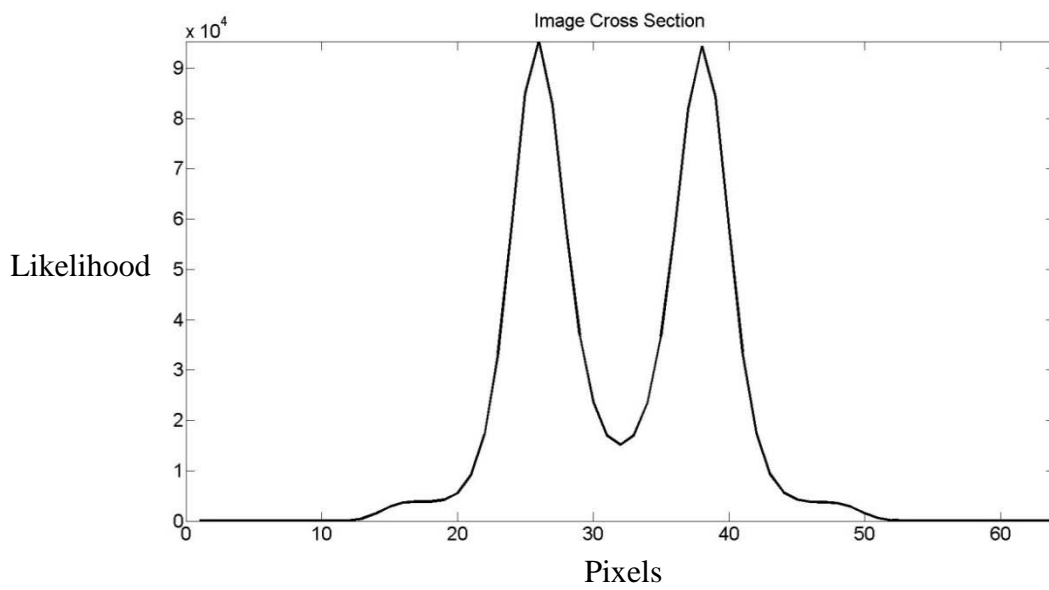Figure 4.2: A cross section of the object shown in Figure 4.1

Figure 4.3: An example of the reconstructed bar target. In this case, the algorithm was easily able to distinguish two different objects.
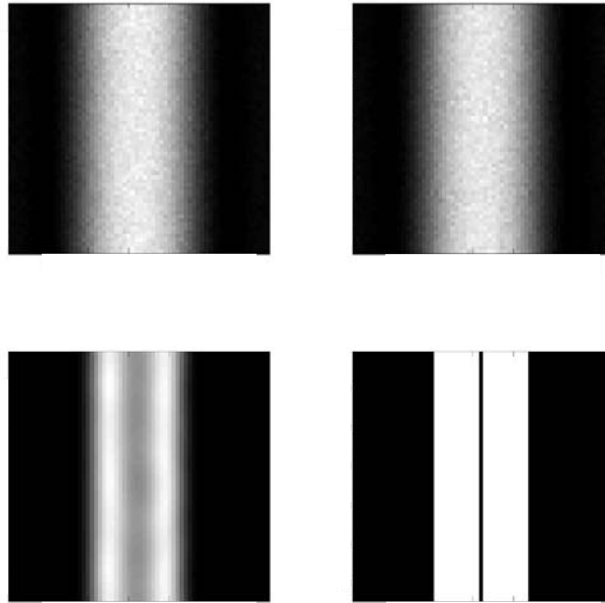
Figure 4.4: A screenshot of the algorithm reconstruction the object. The upper left shows the unpolarized data channel, polarized channel in the upper right, object estimate in lower left, and object in lower right.

To characterize how well the individual bars can be resolved, a ratio is taken of the minimum between the two bars and the maximum of the bars. This gives a number less than one with smaller ratios indicating better resolution. To see how different polarizations affect resolution, a contour plot of the ratios is shown in Figure 4.5. The x and y axis are the polarizations of the two bars. The figure shows that the best resolutions are found where at least one of the targets is highly polarized, close to either 0 or 1. The area near zero polarization diversity, along the diagonal, does not fare as well. Along with finding where the best resolutions occur, the average value can be found with respect to the signal level.
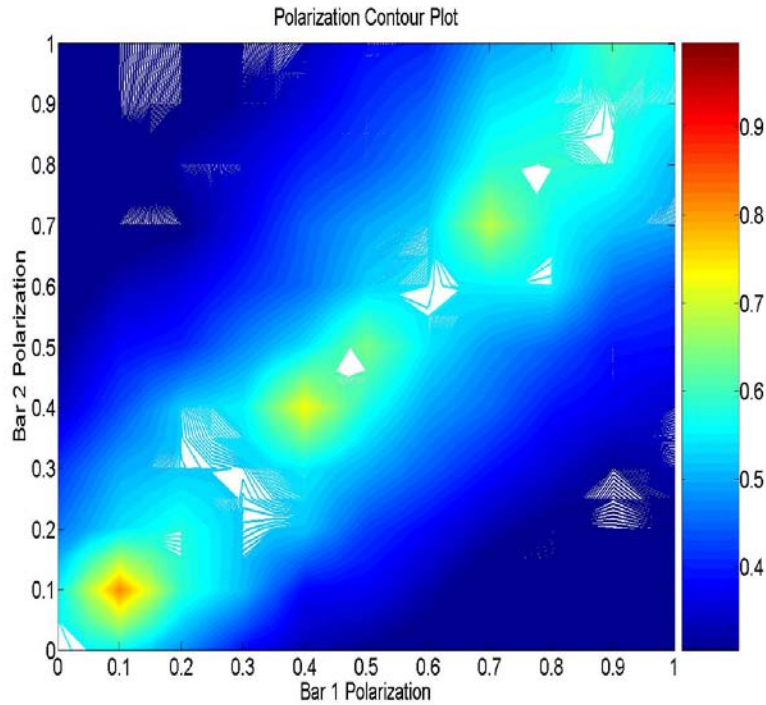
Figure 4.5: An example contour plot of resolving capability based on polarization of bar targets

Test 2: Reproducibility

The next simulation produced the same data as test one but ran only two signal levels, 2×10^4 and 9×10^4 photons, with an r_0 of 3.0cm. The aperture size for all tests was set to 10cm. However, this was repeated 5 times each to make sure that similar, not necessarily identical, contour plots were produced. The 5 contour plots were then averaged. Most of the center areas where there is not much diversity do not show comparatively high resolutions. However, near the very edges where diversity is the highest, the resolutions are much better. This showed that similar results were achieved each time the simulation was initiated.

Test 3: Resolvable Threshold

Through testing a set of different r_0 values, aperture size of 10cm, the threshold at which the algorithm can distinguish two different objects was found to be 2.2cm. At this value, high polarization diversity yields some resolution but not much whereas low diversity still cannot resolve the two objects. If r_0 is incremented to 2.3cm, resolution increases dramatically across all polarization combinations. Figure 4.6 shows a very nice symmetric gradient across all the plots. As the diversity decreases toward the center line, resolution gets worse and then begins to get better as it approaches the other extreme. It should be fairly symmetric since which bar is polarized a certain way shouldn't affect the reconstruction.

The first run of this test was done at a 5×10^4 photocount. Repeating the same simulation with lower signal values of 10^4, 5×10^3, 10^3, and 500 (r_0 of 2.3cm), yields expectedly worse results along the diagonal where there is no diversity. In contrast, as the diversity increases, the signal level becomes less and less important and the reconstruction continues to produce very good results. At a certain point below a photocount of 100, the method for quantifying the data breaks down. The reconstructed image is no longer symmetric. The cross section does not accurately represent the image as a whole.
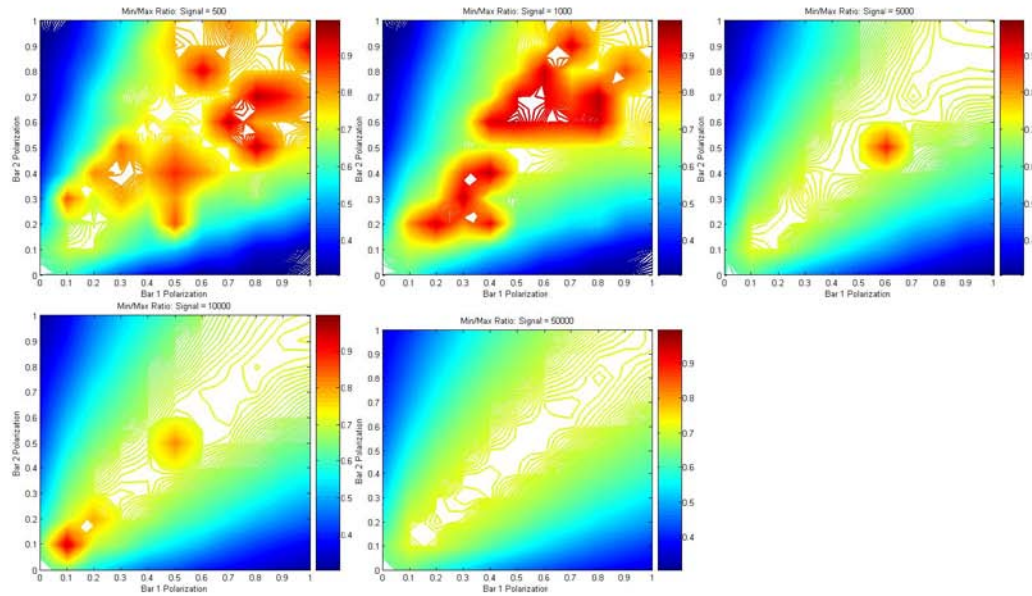
Figure 4.6: Contour plot of resolving capability based on bar polarizations. Signal levels shown are 500 (top left), 1000 (top center), 5000 (top right), 10000 (bottom left), 50000 (bottom right)

Test 4: Sample Satellite Reconstruction

This algorithm was designed to reconstruct images of satellites acquired from ground-based telescopes. In order to make a qualitative estimate of how well the algorithm works, a simulated satellite is used. Figure 4.7 shows the unpolarized satellite and the polarized satellite before propagation. The polarized data was created using an edge detection filter on the unpolarized object to represent the high polarization of edges. This is not the best representation of a polarized satellite but it is sufficient for this test. Figure 4.8 shows another screenshot of the algorithm with both data channels, the object and the reconstruction. There is noticeably better resolution on the reconstruction than the raw data.
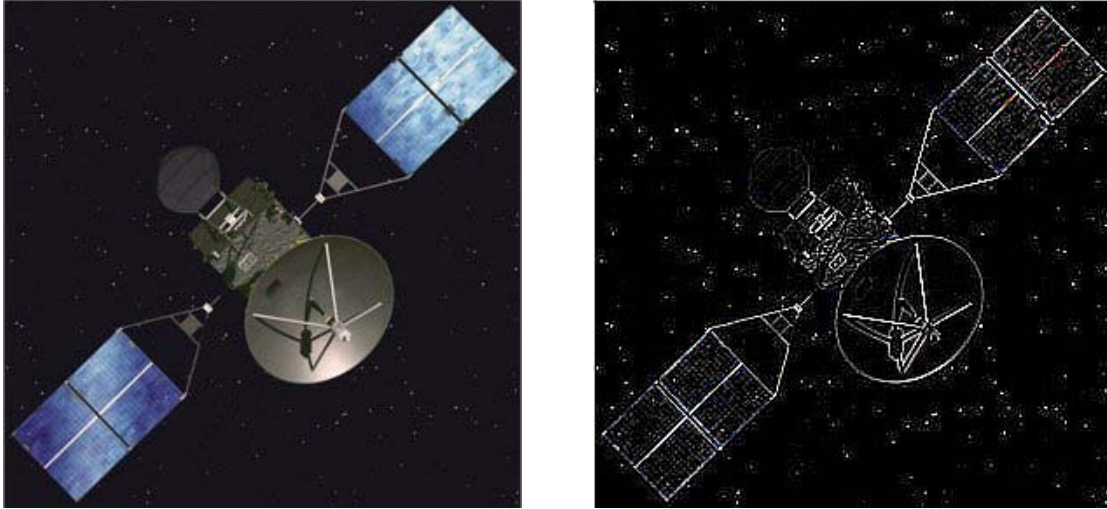
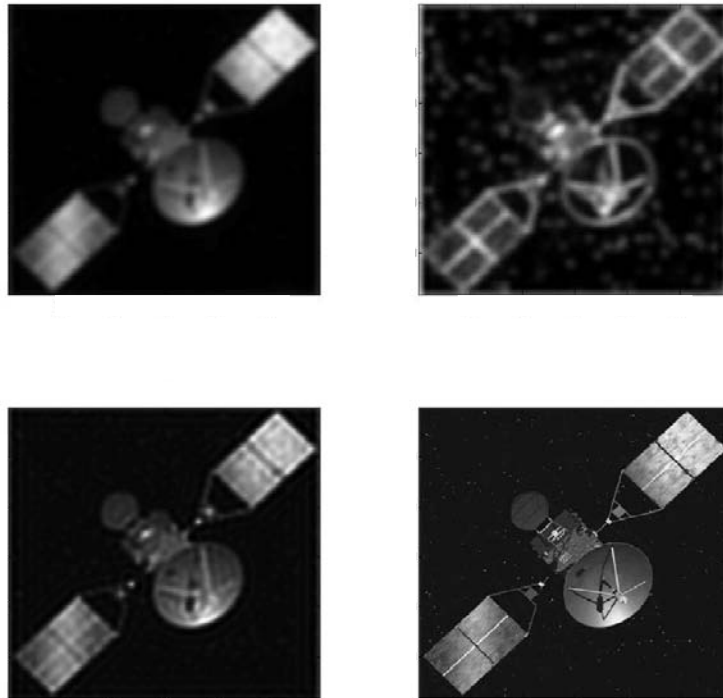Figure 4.7: A satellite with the unpolarized object (left) and polarized object (right)

Figure 4.8: Screenshot of the algorithm restoring a satellite image. Unpolarized data channel (top left), polarized data channel (top right), object estimate (bottom left), object (bottom right)

V. Conclusions

5.1 General Conclusions

The purpose of the algorithm developed in this thesis was to produce improved object estimates beyond that of single channel models currently employed. The process is dependent on not just polarization but polarization diversity. When two points in the image have significantly different polarizations, one horizontal and one vertical for instance, the ability of the algorithm to resolve them is greatly increased. In contrast to this, when there is little to no diversity the algorithm will only resolve as well as a single channel system would.

The first unexpected consequence of using polarization diversity is that it is invariant to signal level. When there is high diversity, low signal levels can be resolved just as well as much higher ones. This continues down to SNR's below 10. However, as the signal decreases, points with low polarization diversity cannot be distinguished as well or at all. The required level of diversity increases as the signal fades. The points must be increasingly polarized to achieve the same resolution but, at the extremes points, they are always resolved to the same high level.

The other goal of the algorithm was to determine the Fried's parameter for the atmosphere without having any knowledge of the seeing conditions. The work done by MacDonald [7:5-(29-30)] required a secondary method to calculate the r_0 value from the likelihood curve. Without a separate estimation of the r_0 value, the likelihood curve rises steeply and levels off but never reaches an apex. In the case of polarization diversity, this additional calculation is not needed. The curve does reach a maximum and then begins to

decrease. With the additional information provided by a two channel system, the correct seeing parameter naturally falls out of the likelihood.

5.2 Future Work

One simulation that was not preformed was to determine the exact resolving capability based on polarization and bar separation. This simulation would show how well or badly the algorithm can resolve compared to the diffraction limit of the optic used. Previous work done by Strong showed that resolutions up to twice the diffraction limit are possible using the polarization diversity method he developed [11].

The system used in this thesis is two-channel, with one unpolarized and one linearly polarized. The algorithm could be expanded to be a multi-channel system incorporating several polarization parameters, including the other linear polarization and both left and right circularly polarized states. Adding in the third channel for the other linear state is relatively easy. The circular polarizations would require a greater effort.

The algorithm has yet to be tested using measured data. A suggested method for a controlled test is to use a small telescope pointed towards a bar target along a horizontal path. Just as a simulated bar target was used in chapter 4, a physical one could be used with a polarizer placed in front of each one of the bars. Using a horizontal path can allow for the average r_0 value to be accurately estimated. Images could then be taken through the telescope and processed using the algorithm in the exact same way that the simulated data was.

Two observatory sites are currently attempting to resolve Geo satellites, University of Arizona MMT, Figure 5.1, and the Maui Space Surveillance Center, Figure 5.2. The algorithm could be tested and implemented for data acquired at these sites. With the notable degree of polarization usually found in reflected light from satellites and the low signal levels from them, it is a prime candidate for this algorithm.

Another possible application is in Solar Physics. The Sun's intense magnetic field has an effect on the light emitted from the solar surface. The Zeeman Effect splits light emitted in strong magnetic fields. A slight shift in wavelength occurs slightly above and below the non-degenerate state. The separate spectroscopic lines are also polarized. This polarization is very noticeable especially in and near sunspot regions. The polarization diversity algorithm can be used to resolve these sunspot features. Due to the high signal levels received from the sun, adaptive optics are not usually feasible in solar observation making this an ideal application [2:150-152,418-419].
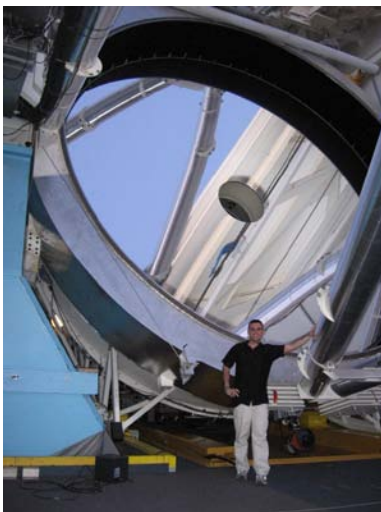

Figure 5.1: 6.5 meter primary telescope mirror at the University of Arizona MMT.

Figure 5.2: Air Force Maui Optical Station. Haleakala, Maui, Hawaii . Image take from AMOS website: http://www.maui.afmc.af.mil/Photos/MSSS2_lg.jpg

Bibliography

[1] Andrews, Larry C. and Ronald L. Phillips. *Laser Beam Propagation Through Random Media* (2nd Edition). Bellingham: SPIE Press, 2005.

[2] Carroll, Bradley W. and Dale A. Ostlie. *An Introduction to Modern Astrophysics*. New York: Addison-Wesley Publishing Company, Inc., 1996.

[3] Committee on Armed Services of the United States Senate and House of Representatives. *Report of the Commission to Asses United States National Security Space Management and Organization.* Pursuant to Public Law 106-65: January 11, 2001.

[4] Dempster, A. P., N. M. Laird, and D. B. Rubin, "Maximum likelihood from incomplete data via the EM algorithm," *J. R. Stat. Soc. B*, 39, 1-37 (1977).

[5] Goodman, Joseph W. *Statistical Optics*. New York: John Wiley & Sons, Inc., 1985.

[6] -----. *Introduction to Fourier Optics* (3rd Edition). Colordad: Roberts & Company Publishers, 2007.

[7] MacDonald, Adam. *Blind Deconvolution of Anisoplanatic Images Collected by a Partially Coherent Imaging System*. Institute of Technology (AU), Wright-Patterson AFB OH, June 2006.

[8] -----, S. Cain, and E. Armstrong, "MAP Image and Seeing Condition Estimation from Partially Coherent 2-D LIDAR Images," *Optical Engineering*, Vol. 45, No. 8, 086201 (August 2006).

[9] Pedrotti, Frank L. and Leno S. Pedrotti. *Introduction to Optics* (2nd Edition). Upper Saddle River: Prentice-Hall, Inc., 1993.

[10] Schultz, Timothy J. "Multiframe blind deconvolution of astronomical images," *J. Optical Society of America A*, Vol. 10, No. 5, 1064-1073 (May 1993).

[11] Stong, David M. *Polarimeter Blind Deconvolution Using Image Diversity*. Air Force Institute of Technology (AU), Wright-Patterson AFB OH, September 2007.

REPORT DOCUMENTATION PAGE

Form Approved
OMB No. 0704-0188

The public reporting burden for this collection of information is estimated to average 1 hour per response, including the time for reviewing instructions, searching existing data sources, gathering and maintaining the data needed, and completing and reviewing the collection of information. Send comments regarding this burden estimate or any other aspect of this collection of information, including suggestions for reducing the burden, to Department of Defense, Washington Headquarters Services, Directorate for Information Operations and Reports (0704-0188), 1215 Jefferson Davis Highway, Suite 1204, Arlington, VA 22202-4302. Respondents should be aware that notwithstanding any other provision of law, no person shall be subject to any penalty for failing to comply with a collection of information if it does not display a currently valid OMB control number.
PLEASE DO NOT RETURN YOUR FORM TO THE ABOVE ADDRESS.

1. REPORT DATE (DD-MM-YYYY)	2. REPORT TYPE	3. DATES COVERED (From - To)
26-03-2009	Master's Thesis	May 2007 - March 2009

4. TITLE AND SUBTITLE	5a. CONTRACT NUMBER
Blind Deconvolution Through Polarization Diversity of Long Exposure Imagery	5b. GRANT NUMBER
	5c. PROGRAM ELEMENT NUMBER

6. AUTHOR(S)	5d. PROJECT NUMBER
James, Steven P, First Lieutenant, USAF	5e. TASK NUMBER
	5f. WORK UNIT NUMBER

7. PERFORMING ORGANIZATION NAME(S) AND ADDRESS(ES)	8. PERFORMING ORGANIZATION REPORT NUMBER
Air Force Institute of Technology Graduate School of Engineering and Management (AFIT/EN) 2950 Hobson Way, Building 640 WPAFB OH 45433-8865	AFIT/EO/ENG/09-06

9. SPONSORING/MONITORING AGENCY NAME(S) AND ADDRESS(ES)	10. SPONSOR/MONITOR'S ACRONYM(S)
Major David Strong Air Force Research Lab Directed Energy Directorate Air Force Maui Optical and Supercomputing Site 535 Lipoa Parkway Suite 200, Kihei, Hawaii. 96753 Phone: (808) 891-7753 Email: David.Strong@maui.afmc.af.mil	AFRL/RDSM
	11. SPONSOR/MONITOR'S REPORT NUMBER(S)

12. DISTRIBUTION/AVAILABILITY STATEMENT

Approved for public release; Distribution unlimited

13. SUPPLEMENTARY NOTES

14. ABSTRACT

The purpose of the algorithm developed in this thesis was to create a post processing method that could resolve objects at low signal levels using polarization diversity and no knowledge of the atmospheric seeing conditions. The process uses a two-channel system, one unpolarized image and one polarized image, in a GEM algorithm to reconstruct the object. Long exposure images were simulated and a simple Kolmogorov model used. This allowed for the atmosphere to be characterized by single parameter, the Fried Parameter. Introducing a novel polarization prior that restricts the polarization parameter, it was possible to determine the Fried Parameter to within half a centimeter without any addition knowledge or processes. It was also found that when high polarization diversity was present in the image could be reconstructed with significantly better resolution and signal level did not affect this resolving capability. At very low signal levels, imagery with low to no diversity could not be resolved at all whereas high diversity resolved equally as well as if there was a high signal level.

15. SUBJECT TERMS

Flash LADAR, laser detection and ranging, range estimation algorithms

16. SECURITY CLASSIFICATION OF:			17. LIMITATION OF ABSTRACT	18. NUMBER OF PAGES	19a. NAME OF RESPONSIBLE PERSON
a. REPORT	b. ABSTRACT	c. THIS PAGE	UU	51	Dr. Stephen C. Cain
U	U	U			19b. TELEPHONE NUMBER (Include area code) (937) 255-3636 x4617 stephen.cain@afit.edu

Reset

Standard Form 298 (Rev. 8/98)
Prescribed by ANSI Std. Z39.18

43